Exploring a free energy landscape by means of multidimensional infrared and terahertz spectroscopies

Yohichi Suzuki[a] and Yoshitaka Tanimura
Department of Chemistry, Graduate School of Science, Kyoto University, Kitashirakawa, Sakyoku, Kyoto 606-8502, Japan

(Received 28 November 2007; accepted 25 February 2008; published online 22 April 2008)

A model for the dipolar crystal system is employed to explore a role of free energy landscape (FEL), in which dipolar molecules are posted on two-dimensional lattice sites with two-state libratinal dynamics. All dipole-dipole interactions are included to have frustrated interactions among the dipoles. For the regular and distorted lattice cases, the FEL is calculated from the interaction energies and the total polarizations for all possible dipolar states at various temperatures. At high temperatures, the shape of the calculated FEL is smooth and parabolic, while it becomes bumpy at low temperatures exhibiting multiple local minima. To study dynamical aspects of the system, the single flip dynamics and the single-double mixed flips dynamics of dipoles are examined from a master equation approach. As the observables of linear absorption and two-dimensional (2D) infrared, far infrared, and terahertz spectroscopies, the first- and third-order response functions of polarization are calculated for different physical conditions characterized by the FEL. While the linear absorption signals decay in time in a similar manner regardless of the FEL profiles, the 2D signals exhibit prominent differences for those profiles. This indicates that we may differentiate the FEL profiles by changing two-time valuables in 2D spectroscopy. As illustrated in the single-double flips case, the FEL study by means of 2D spectroscopy, however, relies on the dynamics which is set independently from the FEL. The Smoluchowski equation is applied to examine the description of the collective dynamics on the microscopically calculated FEL. We found that the one-dimensional and 2D signals calculated from the Smoluchowski equation agree with those from master equation only at temperatures where the FEL becomes parabolic shape. © *2008 American Institute of Physics*. [DOI: 10.1063/1.2897982]

I. INTRODUCTION

Ensembles of atomic or molecular systems with competing interactions exhibit intriguing behaviors. In a glass and an amorphous solid, the long time relaxation processes play a major role as temperature lowered, leading to a slowing down and a broadening in the dynamical response.[1] The incomplete crystallization of polymers due to their topological connectivity and initial configuration makes the polymer chains fold back and forth to form crystalline lamellae.[2] Despite the complex energetics between a reactant and a product along with their surrounding solvent, electron transfer (ET) processes can be well characterized by the inverted parabolic dependence of ET rates as the function of energy gap.[3] Protein molecules fold into precise three-dimensional shapes under the entropic frustration associated with the chain connectivity.[4] Much of this complexity can be described and understood by taking a statistical approach to the energetics of molecular conformation, that is, to free energy landscape (FEL). While the potential energy surface only deals with energetics, the FEL can deal with both the energetics and entropy.[5,6] The FEL concept was introduced by Landau to explain a phase transition between liquid and crystal or between different crystal structures.[7]

The FEL is a conformational substate of the free energy. For a macroscopic variable X, it is defined by

$$F(X) = -k_B T \ln Z(X), \tag{1.1}$$

where

$$Z(X) = \sum_{j \text{ for fixed } X} \exp[-E_j/k_B T] \tag{1.2}$$

is the partition function for the fixed X. The Helmholtz free energy is then expressed as

$$F = -k_B T \ln\left[\int dX Z(X)\right]. \tag{1.3}$$

The function $F(X)$ is regarded as the constrained free energy with X. In the Landau case, X is the order parameter that represents the difference between the phases such as liquid and crystal. Although X is convenient to characterize a system with complex interactions, it is not necessary to be a physical variable that can be controlled from external perturbation. The free energy and FEL are defined under the thermal equilibrium, and $\exp[-F(X)/k_B T]$ corresponds to a probability which the macroscopic quantity takes X. If X cannot be controlled externally, $F(X)$ becomes merely a formal expression that can be used for theoretical analysis only. Nevertheless, the FEL plays an important role to discuss critical phenomena[8] because its definition contains the ther-

[a]Electronic mail: yohichi@kuchem.kyoto-u.ac.jp.

mal fluctuation. The basic assumption of this argument is that the system prefers to take the energy minimal of $F(X)$ from other metastable states. Each state in different phases is explained by a local minimal point of $F(X)$, such as $F(X=1)$ for liquid and $F(X=0)$ for solid. While we explore the landmarks rather than the landscape of $F(X)$ in the case of phase transition, we survey the entire FEL for relaxation dynamics. A time-dependent Ginzburg–Landau (TDGL) approach, that assumes a driving force of X to be proportional to $dF(X)/dX$, is such an example. This formalism was introduced to investigate dynamical phenomena of superconductors[9] and was also used to explain a motion of domain walls or interfaces.[10,11]

As the TDGL approach was used to study critical phenomena, FEL became an important theoretical tool to analyze ET reaction problems.[3] In the ET case, a reaction coordinate could be adequately defined by the microscopic interaction energy,[12] and a number of computer simulations were carried out to confirm the legitimacy of Marcus's theory.[13–16] The dynamics of ET processes was also investigated by using a Smoluchowski-type equation for FELs of the reactant and product states.[17–23] At the present time, the FEL for ET processes is fairly understood at least for the high temperature case, where the FEL is characterized by a simple parabolic shape and the interest of researchers shift to a low temperature case, where the solvent motion freezes.[24–29]

In general, the FEL at high temperature is characterized by a simple parabolic shape; a system with involving complex interaction networks shows complex FEL at low temperature depending on a choice of X. Examples such as a spinglass,[8] glass,[30,31] atomic cluster,[32] polymers,[33,34] and proteins,[35–40] indicate that a full understanding of the dynamical process requires a global overview of the FEL. Such system exhibits many basins corresponding to metastable states, and the dynamics among basins is believed to govern the dynamical properties of materials. Special attentions were paid for protein folding problems, where the energy landscapes of protein have a single dominant basin and an overall funnel topography.[41,42]

Although the FEL analysis is proven to be a useful theoretical framework and is widely used to discuss structures and dynamics of complex systems, there are fundamental difficulties especially to investigate the dynamics at low temperature. Most of difficulties arise from the calculations of the FEL, because even in a small system, an enormous number of states need to be generated. For instance, for a fifty two-level spins system, more than 10^{15} states must be generated for the calculation which cannot be handled by present computers. Several sampling methods were developed to simulate the FEL for the large systems,[43,44] however, the sampling procedure may truncate the dynamical pathways of the system and may change the dynamical aspects especially at low temperature.

The nature of FEL itself also raises a fundamental question because the systems with different dynamics can have the same FEL. For example, if the system dynamics is described by either the Langevin dynamics[45] or MC (Glauber dynamics),[46] their FELs are the same as long as the system part of the Hamiltonian is the same. Since the FEL is defined by the equilibrium state where dynamical behaviors become invisible, it is possible to consider the FEL and the dynamics are independent issues of discussions. From experimental side, it is difficult to justify the validity of FEL theory, since the FEL itself is not experimentally observable and, in addition, X is usually not the experimentally controllable variable. A number of issues related to the dynamical properties on FEL have been postulated. One of our aims in this paper is to clarify some of postulation used to describe the dynamics on FEL at low temperature.

We have employed a simple model to reduce the degrees of freedom as was done for protein[47,48] and solvated ion system.[24–27] We consider a system consists of dipoles[49,50] and employ the model to calculate the FEL at various temperatures by generating all possible states.[29] We depict the FEL as the function of total dipole moments (polarization) which is the macroscopic observable of the system. We monitor the dynamics not only by linear absorption spectroscopy but also by multidimensional spectroscopy,[51–53] which is the optical counterpart of multidimensional NMR that can sensitively probe the dynamical aspect of molecules such as mode-mode coupling[54–57] and dephasing mechanisms.[58–62] The sensitivity of two-dimensional (2D) spectroscopy is utilized to characterize the dynamics on different FELs. Here, we calculate 2D signals corresponding to infrared (IR), far IR,[63] or terahertz spectroscopy[64] defined by the four-body correlation functions of dipole operators.

The outline of the paper is as follows. In the next section we briefly explain our simulation model and procedure to calculate FEL. In Sec. III, we set up the master equations for the present model corresponding to the single flip and single-double mixed flips dynamics. The procedures to calculate linear absorption and third-order 2D signals are also explained in this section. We present the calculated FEL in Sec. IV. The one-dimensional (1D) and 2D signals calculated from the microscopic master equation approach and their analysis are given in Sec. V. We compare our microscopic results with the signals calculated from the phenomenological Smoluchowski equation approach in Sec. VI. We close with our conclusions in Sec. VII.

II. SIMULATION MODEL

We start by assuming regular and distorted 2D lattice models for dipolar molecules, which is an extension of our formally used models developed to analyze the energy landscape.[24,26,28,29] The position of each dipole is given by $\mathbf{r}_j=\mathbf{a}_j+\delta\mathbf{a}_j$, where $\mathbf{a}_j$ is the jth lattice point vector and $\delta\mathbf{a}_j$ is the random displacement from lattice point. The jth dipole is described by the angle θ_j and the fixed dipole strength μ; that dipole moment is then expressed as $\mu\mathbf{S}_j(\theta_j)$, where $\mathbf{S}_j(\theta_j)=(\cos\theta_j,\sin\theta_j)$ is the unit vector of the dipole moment. All dipoles interact through the dipole-dipole interaction expressed in the set of angels $\boldsymbol{\theta}=\{\theta_j\}$ as

$$E(\boldsymbol{\theta})=\mu^2\sum_{j=2}^{N}\sum_{k=1}^{j-1}h_{jk}(\theta_j,\theta_k), \tag{2.1}$$

where

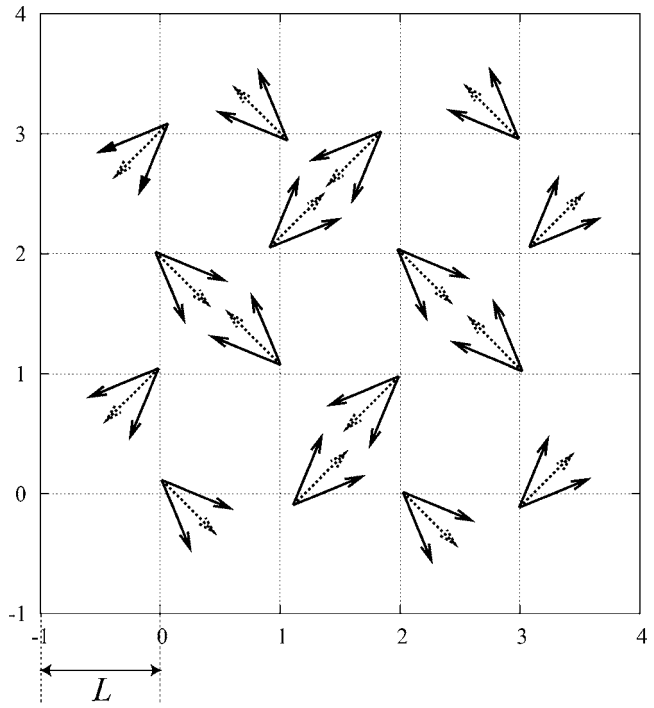

FIG. 1. The Schematic view of a model for representing dipolar molecules. Dipoles are located on the distorted lattice sites and interact through the dipole-dipole interactions. Each dipole is allowed to point two directions (solid arrows) to represents the librational fluctuations. The dotted arrows represent the centers of librational motions, which are obtained from the energy minimum of the four state dipole model.

$$h_{jk}(\theta_j,\theta_k)=\frac{\mathbf{S}_j(\theta_j)\cdot\mathbf{S}_k(\theta_k)|\mathbf{r}_{jk}|^2-3(\mathbf{S}_j(\theta_j)\cdot\mathbf{r}_{jk})(\mathbf{S}_k(\theta_k)\cdot\mathbf{r}_{jk})}{|\mathbf{r}_{jk}|^5}, \tag{2.2}$$

with $\mathbf{r}_{jk}=\mathbf{r}_j-\mathbf{r}_k$ and N is the total number of dipoles. Although this model is intensely simplified, it still contains enormous degrees of freedom and is impossible to evaluate the FEL. Since we are interested in a motion of the system at low temperatures, we may reduce the degrees of freedom by choosing a small subset of states near the lowest energy configuration. We thus construct a further simplified model with the following two steps. We first restrict each dipole to point only four directions $\theta_j=(2n-1)\pi/4$ $(n=1\sim4)$ and find the energy minimum configuration denoted by $\boldsymbol{\theta}^0=\{\theta_j^0\}$ by generating all configurations of $\boldsymbol{\theta}$ (dotted arrows in Fig. 1). Using this minimum configuration, we then construct a two-state dipolar model by adding the two values of the angular shifts $\delta\theta_j=\pm\pi/8$ to each θ_j^0, as depicted by the solid arrows in Fig. 1. This model simulates the librational fluctuations around the energy minimum. We set $\delta\theta_j=\pm\pi/8$ to have a discretized expression of a macroscopic variable (i.e., an order parameter or a reaction coordinate) for the FEL. This model may be oversimplified to study a real system, but it should be sufficient to grasp a relation between the FEL and dynamics.

From Eqs. (2.1) and (2.2), the total energy of our model is written as $E(\boldsymbol{\theta}^0+\delta\boldsymbol{\theta})$, where the set of angular shifts is defined by $\delta\boldsymbol{\theta}=\{\delta\theta_j\}$. We set $\mu=1.85$ and $L=1$ in the units of Debye and 2.1 Å, respectively, as the typical of dipolar liquid. The characteristic energy is then evaluated as $\Delta U=1.08\times10^{-20}$ J, which is about $2.5(k_BT)$ at room temperature. The displacements from the lattice points obey a Gaussian distribution with average $\langle\delta\mathbf{a}_j\rangle=0$ and standard deviation $\langle\delta\mathbf{a}_j^2\rangle$. We chose two parameters for 4×4 lattice corresponding to the structural disorder case $\langle\delta\mathbf{a}_j^2\rangle=0.1$ and the regular lattice case $\langle\delta\mathbf{a}_j^2\rangle=0$. We utilize the open boundary condition to avoid undesired effects that arise from a treatment of boundary.

To study the FEL by means of experiments, we depict the FEL as the function of an experimental observable. Here, the reaction coordinate or the order parameter is chosen to be the total polarization defined by

$$P=\sum_{j=1}^{N}\mu_j^y=\mu\sum_{j=1}^{N}\sin(\theta_j^0+\delta\theta_j), \tag{2.3}$$

where μ_j^y is the jth dipole moment for the vertical direction. Since θ_j^0 can take only $\theta_j=(2n-1)\pi/4$ and we chose $\delta\theta_j=\pm\pi/8$, P takes discrete $N+1$ values for N dipolar system with the constant step size $\Delta P=\sqrt{2}\mu\sin(\pi/8)$. If $N_+(N_-)$ is the number of dipoles whose θ_j^0 satisfies $0\leqslant\theta_j^0<\pi(\pi\leqslant\theta_j^0<2\pi)$, the minimum and maximum values of the reaction coordinate become $P_{\min}=\mu(\sin(\pi/8)N_+-\sin(3\pi/8)N_-)$ and $P_{\max}=\mu(\sin(3\pi/8)N_+-\sin(\pi/8)N_-)$, respectively. For our model, N_+ and N_- satisfy $N_+=N_-=N/2$ because the systems are symmetric with the exclusion of the small deviated positions of dipoles. The values of P are expressed by introducing an integer k which meets $-N/2\leqslant k\leqslant N/2$ in a symmetric form as

$$P(k)=k\sqrt{2}\mu\sin\left(\frac{\pi}{8}\right). \tag{2.4}$$

The FEL is then given by

$$F(P(k))=-k_BT\ln\sum_{i=1}^{2^N}\delta_{P(k),P_i}\exp\left(-\frac{E_i}{k_BT}\right), \tag{2.5}$$

where P_i and E_i are the polarization and energy for the ith state, respectively, and $\delta_{a,b}$ is Kronecker's delta. We denote the polarization for the ith state by P_i and the reaction coordinate specified by an integer k by $P(k)$.

III. DYNAMICS AND OBSERVABLE OF DIPOLAR SYSTEM

A. Master equations for single flip and single-double flips dynamics

First we should point out that our system is not kinetic, since our Hamiltonian is specified by the configurations of the discretized dipoles and does not have a kinetic term. To yield the time evolution, we assume stochastic dynamics among the dipole states that brings the system to be in the thermal equilibrium state at $t\to\infty$. We do not use a kinetic Monte Carlo (MC) approach introduced by Glauber,[46] since we must study dynamics at very low temperature, where the MC sampling does not work properly. Taking an advantage of a small system, we use the master equation approach for all 2^N dipolar states. Since the master equation employs a probability distribution function and does not rely on the

sampling procedure, we can numerically calculate the time evolution of the system at the same CPU time regardless of temperature. We ordered 2^N states as $E_1<E_2<\cdots<E_{2^N}$, where E_k is the interaction energy evaluated from Eq. (2.1) for the kth lowest energy state $\boldsymbol{\theta}^0+\delta\boldsymbol{\theta}_k$. The polarization of $\delta\boldsymbol{\theta}_k$ is evaluated from Eq. (2.3) and is expressed as P_k. We denote the probability distribution for all states by vector $\boldsymbol{\rho}(t)=[\rho_1(t),\rho_2(t),\ldots,\rho_{2^N}(t)]^t$. This master equation is a rate equation for the probability distributions and is expressed as

$$\frac{\partial}{\partial t}\boldsymbol{\rho}(t)=-\mathbf{L}\boldsymbol{\rho}(t), \tag{3.1}$$

where $-\mathbf{L}$ is the transition matrix, whose element $(-\mathbf{L})_{kl}$ describes the transition probability between the lth and kth states. We introduce the polarization vector given by $\mathbf{P}=\Sigma_k P(k)\mathbf{D}_{P(k)}$, where

$$\mathbf{D}_{P(k)}=[\delta_{P(k),P_1},\delta_{P(k),P_2},\delta_{P(k),P_3},\ldots,\delta_{P(k),P_{2^N}}]^t. \tag{3.2}$$

The operator $\mathbf{D}_{P(k)}$ allows us to calculate the probability to have the polarization $P(k)$ from the probability distribution function $\boldsymbol{\rho}(t)$. The total polarization is then expressed as

$$P(t)=\mathbf{P}\cdot\boldsymbol{\rho}(t), \tag{3.3}$$

where the dot represents the inner product.

As was mentioned in Sec. I, the FEL may be the same for the same system with different dynamics. To illustrate this point, we consider two cases of $-\mathbf{L}$ that can be specified by the connectivity coefficient of dipolar states. Consider the qth lowest energy state $\delta\boldsymbol{\theta}_q$. Suppose if we flip a dipole and energy becomes E_p, the connectivity coefficients are specified as $C^{(1)}_{p,q}=1$. Letting p'th states be unreachable from qth state with a single dipole flipping, the coefficients satisfy $C^{(1)}_{p',q}=0$ for the single flip case. If the state is in the qth lowest energy state $\delta\boldsymbol{\theta}_q$ and if the energy becomes E_p with a two-dipolar flipping, we set $C^{(2)}_{p,q}=1$ and $C^{(2)}_{p',q}=0$ for unreachable p'th state for the double flip case. The connectivity coefficients for n flipping of dipoles $C^{(n)}_{p,q}$ can also be defined accordingly. In MC approach, $n=1$ corresponds to the single flip sampling per one MC step yielding the Glauber dynamics,[46] whereas $n=2$ corresponds to the double flip sampling. Since $-\mathbf{L}$ has to satisfy the detail balance condition, transition matrixes for n flipping dynamics have to be in the form of

$$(-\mathbf{L}^{(n)})_{i,j}=\begin{cases} C^{(n)}_{i,j}\exp(-\Delta\tilde{E}_{i,j}/k_BT), & \text{for } \tilde{E}_i>\tilde{E}_j \\ C^{(n)}_{i,j}, & \text{for } \tilde{E}_i<\tilde{E}_j, \end{cases} \tag{3.4}$$

where $\Delta\tilde{E}_{i,j}$ is the energy difference between ith and jth states, i.e., $\Delta\tilde{E}_{i,j}=\tilde{E}_i-\tilde{E}_j$. Here, we consider the linear combination of $n=1$ and 2 flippings defined by

$$-\mathbf{L}=-\alpha\mathbf{L}^{(1)}-\beta\mathbf{L}^{(2)} \tag{3.5}$$

to discuss the different dynamics by a choice of the constants α and β.

B. Laser-system interactions

To calculate response functions, we need to implement an external perturbation based on physical considerations, since our model is not kinetic system. When we apply an external field B to the system, the total energy of the system increases as $-P_jB$ for the jth state. If B is small enough, we can expand the transition matrix for the total Hamiltonian in terms of B. For the single flip case $n=1$, this is written as

$$\frac{\partial}{\partial t}\boldsymbol{\rho}(t)=(-\mathbf{L}^{(1)}+B\boldsymbol{\mu})\boldsymbol{\rho}(t), \tag{3.6}$$

where $\boldsymbol{\mu}$ is the dipolar interaction whose elements are given by

$$\boldsymbol{\mu}_{i,j}=\begin{cases} (-\mathbf{L}^{(1)})_{i,j}\Delta P_{i,j}/k_BT, & \text{for } i>j \\ 0, & \text{for } i<j, \end{cases} \tag{3.7}$$

with $\Delta P_{i,j}=P_i-P_j$. As discussed for $-\mathbf{L}$, we may define the excitation for any flipping number n. As we need to excite the system in the same manner to study the effects of different time evolutions, we consider the single flip excitation case only.

C. First-and third-order response functions

The optical observable of the system is expressed as the response functions of dipole moment or polarization.[65] For the first-order linear and third-order 2D IR, far IR, and terahertz spectroscopies, the signals are expressed in terms of a dipole operator $\hat{\mu}$ as $S(t_1)=i\,\mathrm{tr}\{\hat{\mu}\hat{G}(t_1)(\hat{\mu}^\times\hat{\rho}_{\mathrm{eq}})\}/\hbar$ and $S(t_3,0,t_1)=i^3\,\mathrm{tr}\{\hat{\mu}\hat{G}(t_3)\hat{\mu}^\times[\hat{\mu}^\times\hat{G}(t_1)(\hat{\mu}^\times\hat{\rho}_{\mathrm{eq}})]\}/\hbar^3$,[53] where $\hat{\rho}_{\mathrm{eq}}$ is the equilibrium distribution and we define $i\hat{A}^\times\hat{B}/\hbar\equiv i[\hat{A},\hat{B}]/\hbar$ in the quantal case[66–69] or $i\hat{A}^\times\hat{B}/\hbar\equiv\{\hat{A},\hat{B}\}$ in the classical case.[70] By using the quantal or classical Liouville operator of the system $\hat{L}$, the time-evolution operator is expressed as $\hat{G}(t)\hat{A}\equiv e^{-\hat{L}t}\hat{A}$. For the present case of the master equation, the response functions are expressed as

$$S(t_1)=\sum_k P(k)H_{\boldsymbol{\mu}}(P(k),t_1) \tag{3.8}$$

and

$$S(t_3,0,t_1)=\sum_k P(k)H_{\boldsymbol{\mu}\boldsymbol{\mu}\boldsymbol{\mu}}(P(k),t_3,0,t_1), \tag{3.9}$$

where

$$H_{\boldsymbol{\mu}}(P(k),t_1)=\mathbf{D}_{P(k)}\cdot\exp[-\mathbf{L}t_1]\boldsymbol{\mu}\boldsymbol{\rho}_{\mathrm{eq}} \tag{3.10}$$

and

$$H_{\boldsymbol{\mu}\boldsymbol{\mu}\boldsymbol{\mu}}(P(k),t_3,0,t_1)=\mathbf{D}_{P(k)}\cdot\exp[-\mathbf{L}t_3]\boldsymbol{\mu}\boldsymbol{\mu}\times\exp[-\mathbf{L}t_1]\boldsymbol{\mu}\boldsymbol{\rho}_{\mathrm{eq}}. \tag{3.11}$$

The vector $\boldsymbol{\rho}_{\mathrm{eq}}$ represents the thermal equilibrium distribution whose component is defined by

$$(\boldsymbol{\rho}_{\mathrm{eq}})_i=\exp(-E_i/k_BT)/Z, \tag{3.12}$$

in which Z is the partition function. Analogous to a quantal case,[53] the right-hand side of Eqs. (3.10) and (3.11) can be read from the right to left as follows. The total system is

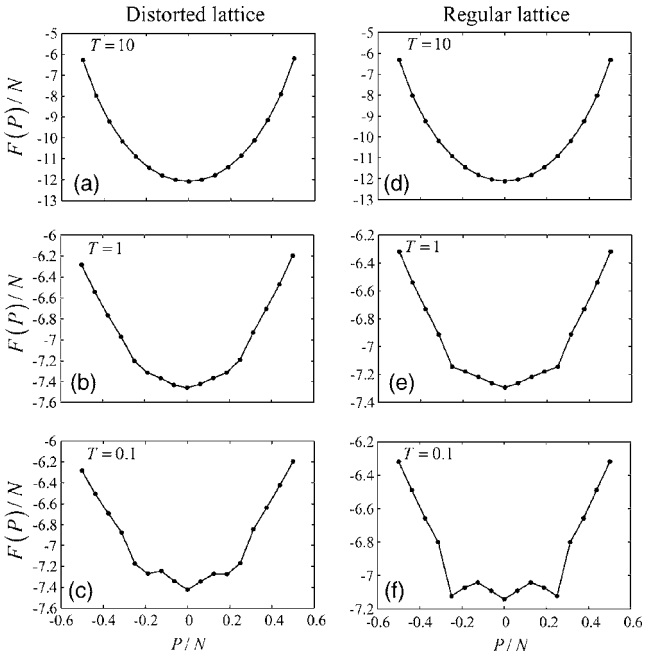

FIG. 2. The FELs as the function of the polarization P in the case of 4×4 distorted and regular lattices at various temperatures: (a) $T=10$, $\langle\delta\mathbf{a}_j^2\rangle=0.1$; (b) $T=1$, $\langle\delta\mathbf{a}_j^2\rangle=0.1$; (c) $T=0.1$, $\langle\delta\mathbf{a}_j^2\rangle=0.1$; (d) $T=10$, $\langle\delta\mathbf{a}_j^2\rangle=0$; (e) $T=1$, $\langle\delta\mathbf{a}_j^2\rangle=0$; and (f) $T=0.1$, $\langle\delta\mathbf{a}_j^2\rangle=0$.

initially in the equilibrium state $\boldsymbol{\rho}_{\mathrm{eq}}$. The initial state is then modified by the first laser pulses via the dipole operator as $\boldsymbol{\mu}$ at $t=0$ and is propagated for time t_1 by $\exp[-\mathbf{L}t_1]$. The probability distribution functions is now given by $\exp[-\mathbf{L}t_1]\boldsymbol{\mu}\boldsymbol{\rho}_{\mathrm{eq}}$. The linear absorption (1D) signal is the expectation value of polarization given by $\Sigma_k P(k)H_{\boldsymbol{\mu}}(P(k),t_1)$. In the third-order 2D measurements, after the first excitation and time evolution for t_1, the system is further excited by the second and third dipole interactions expressed as $\boldsymbol{\mu}\boldsymbol{\mu}$. After these excitations, the system is propagated for the time period t_3 by $\exp[-\mathbf{L}t_3]$ as $\exp[-\mathbf{L}t_3]\boldsymbol{\mu}\boldsymbol{\mu}\exp[-\mathbf{L}t_1]\boldsymbol{\mu}\boldsymbol{\rho}_{\mathrm{eq}}$ and, finally, the expectation value of the dipole moment at t_1+t_3 is obtained by $\Sigma_k P(k)H_{\boldsymbol{\mu}\boldsymbol{\mu}\boldsymbol{\mu}}(P(k),t_3,0,t_1)$. By using the above procedure, we can calculate 1D and 2D signals from the master equation approach.

IV. FELs

In Fig. 2, we illustrate the FELs in the case of 4×4 distorted and regular lattice at various temperatures: (a) $T=10$, $\langle\delta\mathbf{a}_j^2\rangle=0.1$; (b) $T=1$, $\langle\delta\mathbf{a}_j^2\rangle=0.1$; (c) $T=0.1$ $\langle\delta\mathbf{a}_j^2\rangle=0.1$; (d) $T=10$, $\langle\delta\mathbf{a}_j^2\rangle=0$; (e) $T=1$, $\langle\delta\mathbf{a}_j^2\rangle=0$; and (f) $T=0.1$, $\langle\delta\mathbf{a}_j^2\rangle=0$. Here and after, we set $k_B=1$. We analyze the temperature dependence of the heat capacity and find a sharp peak $T_c\approx1$ that are corresponded to the freezing temperature of dipolar librational motions. Therefore the cases for (c) and (f) are in the glassy state. These landscapes are directly calculated from Eq. (2.5) by generating all possible dipolar states numerically.

To elucidate a profile for each of the FELs, we introduce the density of states as the function of $P(k)$, and E is expressed as

$$n(P(k),E)dE=\Omega(P(k))g(P(k),E)dE, \tag{4.1}$$

where $g(P(k),E)$ is the distribution of the density of state between E and $E+dE$ for fixed $P(k)$ and $\Omega(P(k))$ is the total number of states for $P(k)$ defined by

$$\Omega(P(k))=\sum_{r=|k|}^{N/2}{}_{N/2}C_{rN/2}C_{r-|k|}=\frac{N!}{(N/2+|k|)!(N/2-|k|)!}. \tag{4.2}$$

From Eq. (4.1), the FEL given by Eq. (2.5) is evaluated as

$$F(P(k))=-k_BT\ln\int dEg(P(k),E)\times\exp(-E/k_BT)-TS^*(P(k)), \tag{4.3}$$

where $S^*(P(k))=k_B\ln\Omega(P(k))$ is the configuration entropy given by

$$S^*(P(k))\simeq-k_BN\left[\left(\frac{1}{2}+\frac{|k|}{N}\right)\ln\left(\frac{1}{2}+\frac{|k|}{N}\right)+\left(\frac{1}{2}-\frac{|k|}{N}\right)\ln\left(\frac{1}{2}-\frac{|k|}{N}\right)\right]. \tag{4.4}$$

If we assume the energy distribution $g(P(k),E)$ obeys Gaussian form with the central energy $\bar{E}(P(k))$ and the standard deviation $\Delta E(P(k))$, Eq. (4.3) is evaluated as

$$F(P(k))=\bar{E}(P(k))-\frac{\Delta E^2(P(k))}{2k_BT}-TS^*(P(k)). \tag{4.5}$$

The profile of the FEL is governed by the configuration entropy $S^*(P(k))$ at high temperature. By expanding $F(P(k))\approx-TS^*(P(k))$ in power of $|P(k)|$ up to the fourth order, we have

$$\frac{F(P)}{N}\approx-k_BT\left[\ln2-\frac{2}{\Delta P^2}\left(\frac{P}{N}\right)^2-\frac{4}{3\Delta P^4}\left(\frac{P}{N}\right)^4\right], \tag{4.6}$$

where $\Delta P=\sqrt{2}\mu\sin(\pi/8)$. Analogous to the ET case,[29] this result indicates that the profile of the FELs is parabolic for the small P, while an additional quartic contribution to the FEL is found for the large P. Since the quartic term arises from $TS^*(P(k))$, this contribution is attributed to the entorpic origin. In the case of Figs. 2(a) and 2(d), the FEL looks parabolic in the small region of P.

When the temperature drops, the simulated FELs are no longer smooth and a remarkable difference appears between the distorted case [Fig. 2(c)] and the regular case [Fig. 2(f)]. This feature can be explained from the distribution of states as a function of the polarization P and the energy E, as illustrated in Fig. 3. For the regular case, the states are highly degenerated (the close circles in Fig. 3) due to the symmetry of the system, while for the distorted case, the states are not degenerated and irregularly distributed (the open circles in

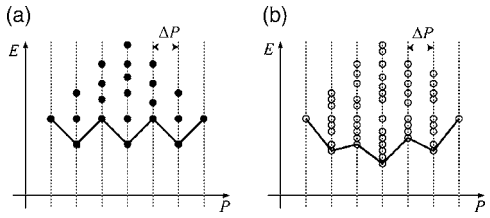

FIG. 3. The schematic pictures of the distribution of states as a function of the polarization P and energy E. The solid line represents FELs for (a) a regular lattice case and (b) a distorted lattice case. The states are highly degenerated due to the symmetry of the system shown as the close circle, while the states are degenerated and irregularly distributed shown as the open circle in (b). As a result, the FEL for the distorted case exhibits prominent irregular profiles.

Fig. 3) because of the frustrated interactions among the dipoles. Since the FELs are determined by the lowest energy states at very low temperature due the Boltzmann factor in Eq. (2.5), the FEL of the distorted lattice exhibits prominent irregular profiles.

V. OPTICAL RESPONSES

A. 1D Signal

Following the procedures explained in Sec. III C, we have calculated the first- and third-order response functions and plotted them as the signals in one- and 2D spectroscopies. In Figs. 4(a)–4(f), the linear absorption (1D) signal $S(t_1)$ for (i) the single-flip case, $\alpha=1$ and $\beta=0$ (solid line), and (ii) the single-double mixed flips case, $\alpha=0.5$ and $\beta=1$ (dashed line), are plotted for the same sets of parameters $\langle \delta \mathbf{a}_j^2 \rangle$ and T used in Figs. 2(a)–2(f), respectively. Although the relaxation rates are different in each case, we find

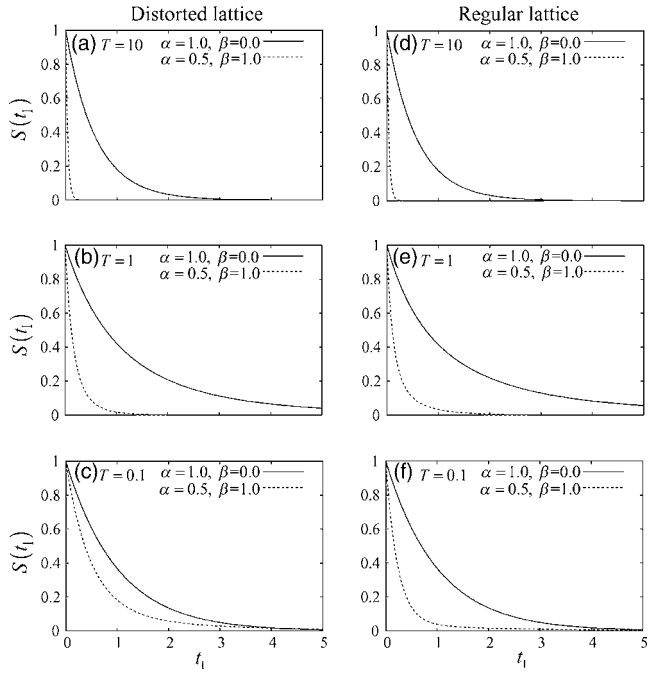

FIG. 4. The linear absorption (1D) signals $S(t_1)$ for (i) single flip case, $\alpha=1$ and $\beta=0$ (solid line), and (ii) single-double mixed flips case, $\alpha=0.5$ and $\beta=1$ (dashed line), are plotted for the same sets of parameters $\langle \delta \mathbf{a}_j^2 \rangle$ and T used in Fig. 2. The intensities of the signals are normalized by their initial values.

that solid and dashed lines in Figs. 4.4.(a) and 4.4(d) at the high temperature are well fitted by a single exponential function, whereas the solid and dashed lines in Figs. 4(b) and 4(e) are fitted by the sum of exponential functions at the intermediate temperature. At the low temperature, the solid lines in Figs. 4(c) and 4(f) are single exponential function, while the dashed lines are represented by the sum of exponential functions.

To investigate these features, we consider a relaxation mode analysis, which utilizes the eigenvalues and eigenmodes of the master equation for a system with complex interactions.[71,72] In this analysis, the time relaxation of a two-body correlation function is characterized by a sum of exponential functions with their decay rates defined by the eigenvalues of the master equation. If the number of the eigenmodes involved in the system is enormous and the eigenvalues are well distributed in the energy space due to the complex interactions in the system, the signal decays nonexponentially, as shown in the case of a 2D ± Ising model at the critical point. Despite the complexity of the interactions between the dipoles, present results decay more or less exponentially regardless of the temperatures. This is because the excitation induced by the laser pulse is highly symmetrical against P and therefore the laser interaction excites only few modes which decay exponentially.

To see this point more closely, we depict $H_{\boldsymbol{\mu}}(P,t_1)$ given in Eq. (3.10) which represents the deviation of the distribution from the equilibrium state after the laser interaction $\boldsymbol{\mu}$ at time $t=0$ for given P. Figures 5(a)–5(f) illustrate the change of $H_{\boldsymbol{\mu}}(P,t_1)$ in time for [(a)–(c)] distorted cases and [(d)–(f)] regular lattice cases at different temperatures in the same order of Figs. 4(a)–4(f) for the single flip dynamics. In each figure, the line above the P axis shows the corresponding FEL. Here, we plot the single flip case only, since the profiles of $H_{\boldsymbol{\mu}}(P,t_1)$ for different temperatures and configurations in the single flip and single-double flips cases are approximately analogous, if we normalized the time scale of each figures by their relaxation rates estimated from Fig. 4. As all figures in Fig. 5 indicate, the primary cause of the signal relaxation is not from the movement of $H_{\boldsymbol{\mu}}(P,t_1)$ toward the $P=0$ point but from the decrease of $H_{\boldsymbol{\mu}}(P,t_1)$ for the fixed position of P. Since $H_{\boldsymbol{\mu}}(P,t_1)$ for the high temperature case in Figs. 5(a) and 5(d) and the very low temperature case in Figs. 5(c) and 5(f) decay monotonically with keeping their profile, we may conclude that the excited states are composed of either the single eigenmode or the eigenmodes that have similar eigenvalues. In the intermediate temperature case in Figs. 5(b) and 5(e), the profile of $H_{\boldsymbol{\mu}}(P,t_1)$ slightly changes as time goes, indicating that those excite states are composed of the eigenmodes with different eigenvalues.

B. 2D Signals

While we could not observe any features specific to the FELs from 1D measurements, we investigate the third-order response function $S(t_3,0,t_1)$. We plot contour maps of 2D signals defined by $S(t_3,0,t_1)$ for the distorted and regular lattice cases at different temperatures in the same order as in Fig. 2. Figure 6 is for single flip ($\alpha=1$, $\beta=0$), while Fig. 7 is

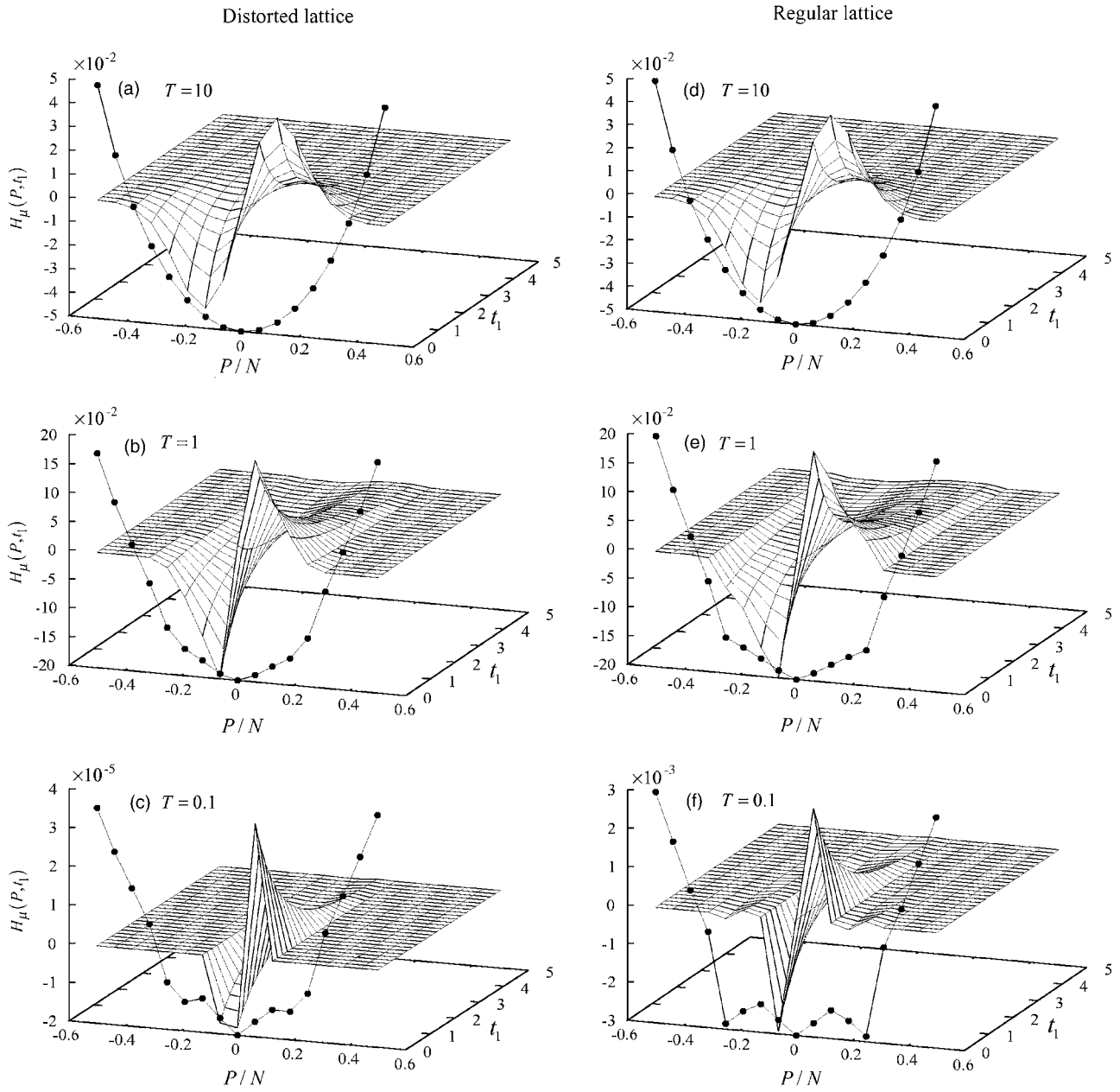

FIG. 5. The time evolution of $H_{\mu}(P,t_1)$ for the single flip dynamics for the distorted cases [(a)–(c)], and the regular cases [(d)–(f)], at different temperatures in the same order of Fig. 2. The line above the P axis shows the corresponding FEL.

for single-double mixed flips (α=0.5, β=1.0) dynamics, respectively. Compared with the 1D case, 2D spectroscopy is much more sensitive to the difference of temperatures, configurations of dipoles, and dynamics. As can be seen in Figs. 2(a) and 2(d), the FELs at the high temperature are similar due to the entropic contributions. The corresponding 2D signals in Figs. 6(a) and 6(d) or Figs. 7(a) and 7(d) show a similar 2D profile, if we normalize the time scales by the relaxation times estimated from Fig. 4. First we should notice that if the dipole element of the laser interaction is a linear function of the system polarization P, the 2D signals will be vanished for a harmonic potential due to the destructive interference of the multiple laser excitations.[53,66,67] Although there is always a quartic anharmonicity in the FEL as illustrated in Eq. (4.6), its contribution is too small to have the signals comparable to the calculated results. In the present case, it is the nonlinearity that causes 2D signals for the high temperature parabolic potential. Based on the profile analysis between the initial equilibrium distribution and the laser excited distribution depicted in Fig. 5, we have found that the effective dipole element in the laser interactions is not linear but linear plus cubic function expressed as $P-\varepsilon P^3$, where ε is the constant in the order of 10^{-2}. The nonlinear contribution arises because we have constructed the dipole operator nonkinetic way by expanding the Liouville operator with the external interaction defined with the Boltzmann factors.

Regardless of the form of the laser interaction, the decays of signal profiles reflect the system dynamics, since the time evolutions of the system between the excitations are governed by the system Liouvillian only. Thus, the 2D profiles in the high temperature case decay monotonically as the

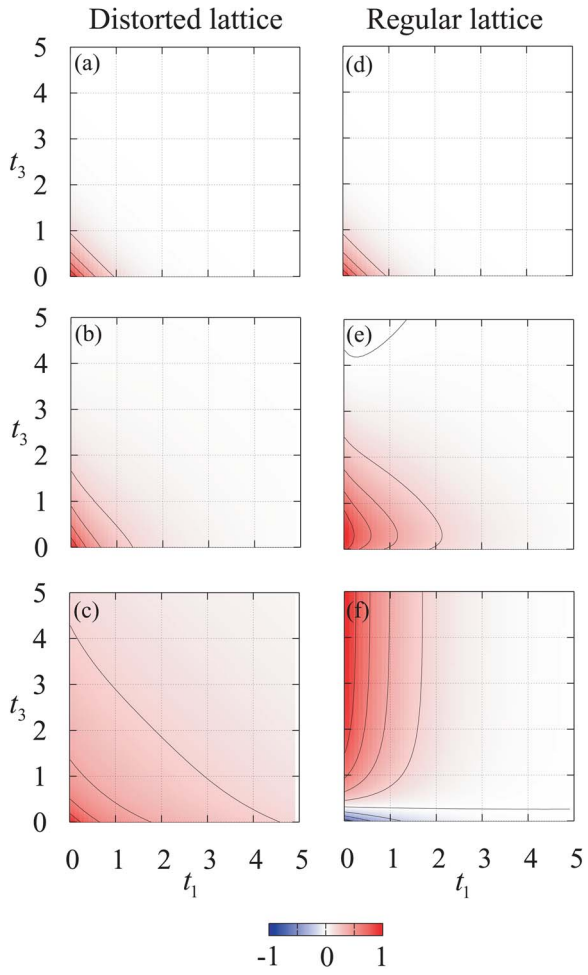

FIG. 6. (Color online) The contour map of the 2D signals for the single flip dynamics. The intensity of each plot is normalized by its maximum or minimum value.

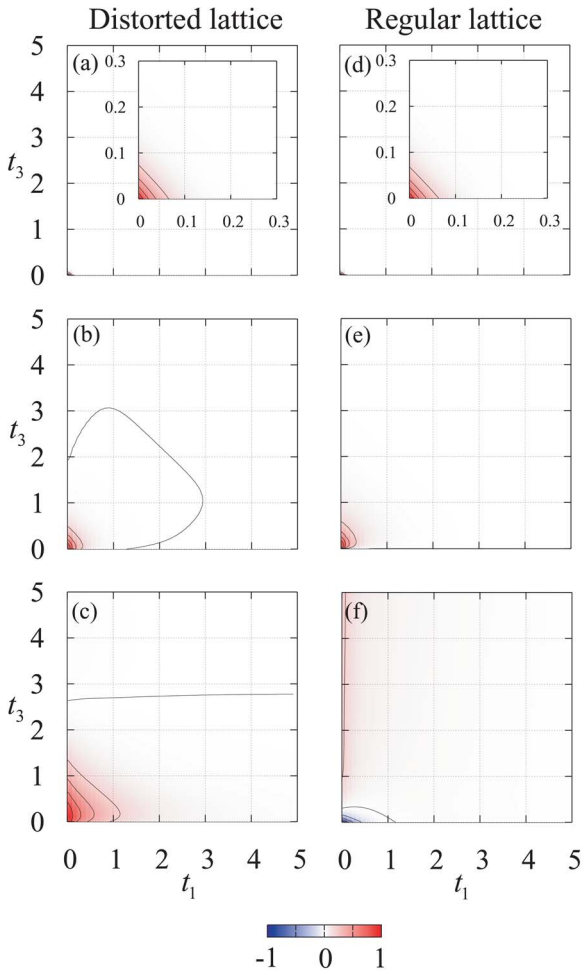

FIG. 7. (Color online) The contour maps of the 2D signals for the single-double mixed flips dynamics (α=0.5, β=1). The intensity of each plot is normalized by its maximum or minimum value. The insets of (a) and (d) show $S(t_3,0,t_1)$ by using the magnified scale.

function of t_1 and t_3. For the intermediate and lower temperature cases as shown in Figs. 2(b), 2(c), 2(e), and 2(f), the anharmonicity of potential is strong, and the primary cause of the signals is the anharmonicity of the FELs rather than the nonlinearly of dipole. While the signals for the distorted and regular cases exhibit similar profiles at high temperature as shown in Figs. 6(a) and (d) and Figs. 7(a) and (d), they show clear differences at low temperature as illustrated in Figs. 6(c) and (f) and Figs. 7(c) and (f). These signals seem to reflect the differences of the FEL profiles presented in Fig. 2, indicating a possibility to detect a profile of FEL. The sensitivity of 2D spectroscopy also suggests a possibility to detect the difference of dynamics on the same FEL, since the profiles depicted in Figs. 6 and 7 are different if the dynamics is different even it is governed by the same FELs.

To see underlying dynamics on 2D signals, we plot the distribution given in Eq. (3.11). Figures 8(a)–8(f) illustrate $H_{\mu\mu\mu}(P,t_3,0,t_1)$ with t_1=0 in the same order as Figs. 2(a)–2(f) for the single flip dynamics, respectively. Although $H_{\mu\mu\mu}(P,t_3,0,t_1)$ is not an observable, it is as sensitive as 2D signals for the difference of dynamics. Thus, $H_{\mu\mu\mu}(P,t_3,0,t_1)$ for the single-double flips case exhibits some differences from the single flip case presented in Fig. 8 unlike the case of 1D spectroscopy. Since a role of FEL can be sufficiently explained from the single flip case, here we display the single flip case only.

For the high temperature cases shown in Figs. 8(a) and 8(d), the distribution profiles decay monotonically, reflecting the monotonic decay of signals observed in Figs. 6(a) and 6(d). Similar behaviors are observed in Figs. 7(a) and 7(d). The difference between Figs. 6(a) and (d) and 7(a) and (d) are their time scales which can be adjusted by the relaxation time estimated from Fig. 4. While the FELs of distorted and regular lattice cases appear similar at the high temperature due to the entropic contribution, they become different at low temperature, which reflects the difference of the system energetics. These differences of FELs seem to be detected by 2D spectroscopy, as illustrated in Figs. 6(b) and 6(e) as well as 7(b) and 7(e). The relaxations of distributions presented in Figs. 8(b) and 8(e) are no longer monotonic because the multiple excitations involved in 2D spectroscopies excite the various modes with different relaxation constants. Since a role of relaxation depends on the time sequence t_1 and t_3, the 2D spectroscopy can provide more information than 1D spectroscopy.

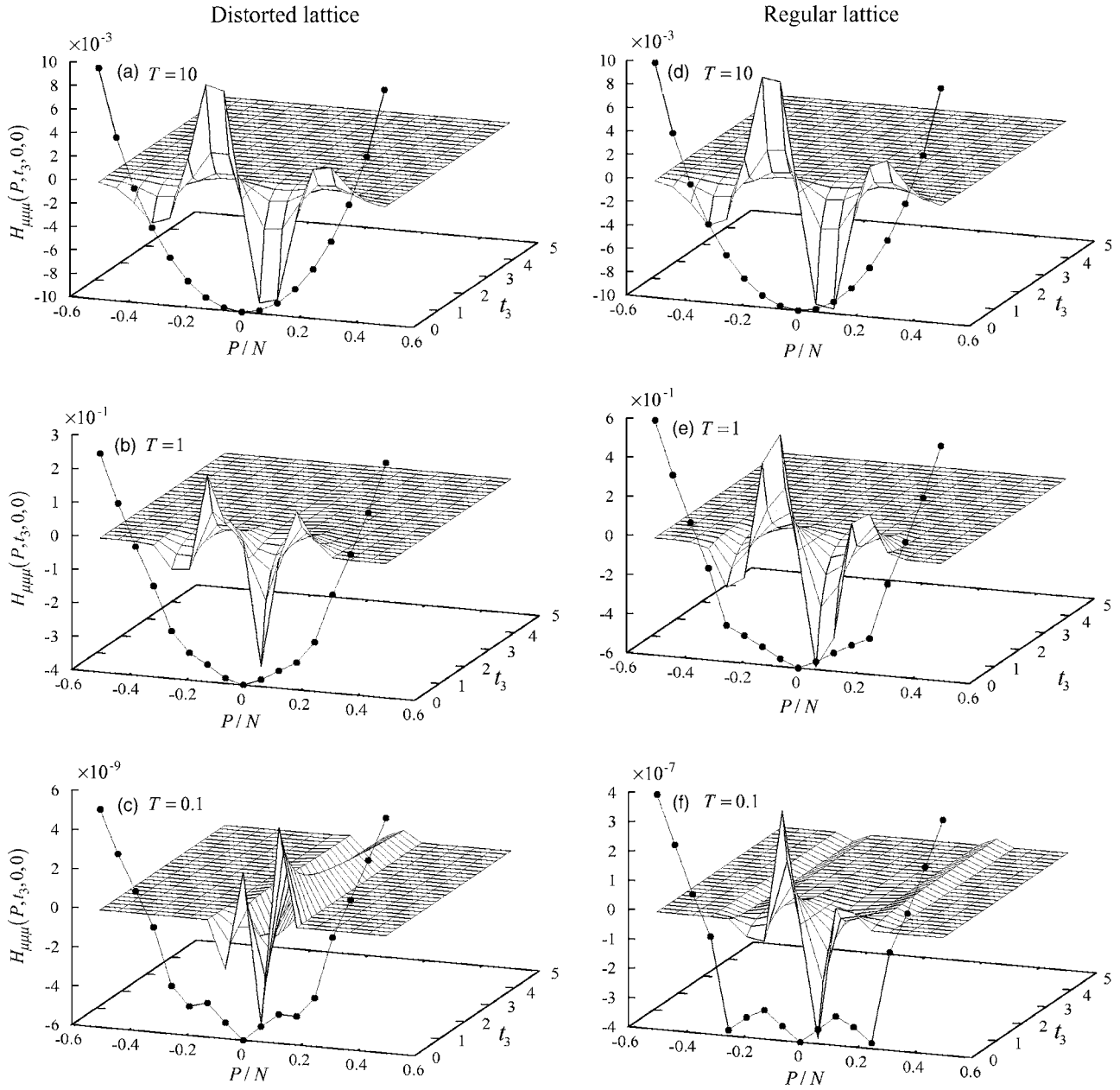

FIG. 8. The time evolution of $H_{\mu\mu\mu}(P,t_3,0,t_1)$ for the single flip dynamics with $t_1=0$ for the distorted cases [(a)–(c)], and the regular cases [(d)–(f)], at different temperatures in the same order of Fig. 2. The line above the P axis shows the corresponding FEL.

When the temperature becomes very low, a remarkable difference appears between the distorted and regular cases. This difference can be easily explained by comparing the time evolution of $H_{\mu\mu\mu}(P,t_3,0,t_1)$, as shown in Figs. 8(c) and 8(f). The elongation of the peak in the t_3 directed in Fig. 6(f) can be attributed to the trapping of the distribution in the local minima around $P/N=\pm 0.25$, as illustrated in Fig. 8(f). We also have observed the trapping of $H_{\mu\mu\mu}(P,t_3,0,t_1)$ in the single-double mixed flips case (not shown), but the trapped distribution decays more quickly than the single flip case and the elongated contribution in Fig. 7(f) is much smaller than that in Fig. 6(f). Since other 2D signals do not show the elongation, this implies that the local minimum of the FEL may be detected as the elongated peak in the t_3 direction in the 2D IR spectroscopy.

VI. SMOLUCHOWSKI EQUATION APPROACH

To discuss dynamical behaviors of FELs, a TDGL equation approach[9–11] and Smoluchowski equation approach[17–23] are often used by assuming a driving force of macroscopic coordinate X which is proportional to the gradient of the free energy $dF(X)/dX$. For a simple model of ET problem, a relationship between the master equation and the Smoluchowski equation approaches has been clarified for the high temperature case,[25] but the validity of such equation of motion approaches for the low temperature case has not been explored. Here, we examine the applicability of the Smoluchowski equation approach by calculating 1D and 2D signals for the FELs given in Figs. 2(a)–2(f) and compared with the microscopically calculated 1D and 2D signals presented in Sec. V.

For the distribution $H(P,t)$, the Smoluchowski equation is expressed as

$$\frac{\partial}{\partial t}H(P,t) = -\mathbf{L}_S H(P,t). \tag{6.1}$$

The Liouville operator is given by

$$-\mathbf{L}_S = D\left[\frac{1}{k_B T}\frac{\partial}{\partial P}\left(\frac{\partial F(P)}{\partial P}\right) + \frac{\partial^2}{\partial P^2}\right], \tag{6.2}$$

where D is the diffusion constant. The Smoluchowski equation describes the same dynamics as the overdamped limit of the Langevin dynamics with the white noise fluctuations. In the Smoluchowski case, the dynamics is described as the probability diffusion on the potential $F(P)$. As discussed in the ET case,[25] one can relate to the microscopic master equation approach and phenomenological Smoluchowski equation approach if the system is in the high temperature case. In Appendix A, we deduce the Smoluchowski equation for the single flip and single-double flips master equations assuming the large system with high temperature. Thus, in the high temperature case, we can estimate the coefficients in Eq. (6.2) directly from the master equation. Note that, as shown in Appendix A, the single flip and single-double flips dynamics of the master equation approach can be treated uniformly in the Smoluchowski equation approach as the choice of diffusion parameters. Since the phenomenological features do not depend on the diffusion parameters, we discuss the single flip case only to examine the validity of Smoluchowski equation.

To calculate 1D and 2D signals, we need to define the dipole operator. As mentioned in Sec. V, the dipole element introduced in the master equation approach contains the cubic polarization term. We consider the free energy with the electric perturbation expressed as $F(P)-B(P+\varepsilon P^3)$, where B is a weak electric field and a small constant. By expanding the free energy by the perturbation up to the first order, we have the dipole operator in the form

$$\boldsymbol{\mu}_S = -\frac{D}{k_B T}\left[\frac{\partial}{\partial P} + \varepsilon\left(6P + 3P^2\frac{\partial}{\partial P}\right)\right], \tag{6.3}$$

where we evaluate $\varepsilon=-0.03$ from the master equation approach. By replacing the Liouvillian and dipole operator in Eqs. (3.10) and (3.11) by Eqs. (6.2) and (6.3), we can calculate the 1D and 2D signals from the Smoluchowski approach. Note that the equilibrium state in the Smoluchowski approach is given by $\rho_{\mathrm{eq}} \propto \exp(-F(P)/k_B T)$. In Figs. 9(a)–9(c), we plot the 1D signals calculated from the Smoluchowski approach for the FELs given in Figs. 2(a)–2(f). In each figure, the solid and dashed lines represent the distorted and regular lattice cases, respectively. The nonlinearlity of the dipole element does not play a major role in the 1D case, since it gives rise to a minor correction of the signals. We adjust the diffusion constants to fit the results from the single flip master equation dynamics. For the high temperature case, we use $D=7.14$ for the distorted and regular lattices, which roughly agrees to the value reduced from the master equation. In the high temperature case in Fig. 9(a) where the FEL profile becomes parabolic, we can analytically evaluate the 1D signals from Smoluchowski approach as described in Appendix B, and the single exponential decay of the signals, which was also observed in the master equation approach, is explained as the relaxation of the harmonic mode. For the intermediate and low temperature cases shown in Figs. 9(b) $T=1$ and 9(c) $T=0.1$, the relaxation constants for the distorted and regular lattices are evaluated as (b) $D=1.67$ (solid line) and $D=2.50$ (dashed line) and (c) $D=0.010$ (solid line) and $D=0.028$ (dashed line). While all curves in Fig. 9(b) can be fitted by a simple exponential function, the curves in Fig. 9(c) are expressed by the sum of exponential functions, which are different from the microscopic results given in Fig. 4.

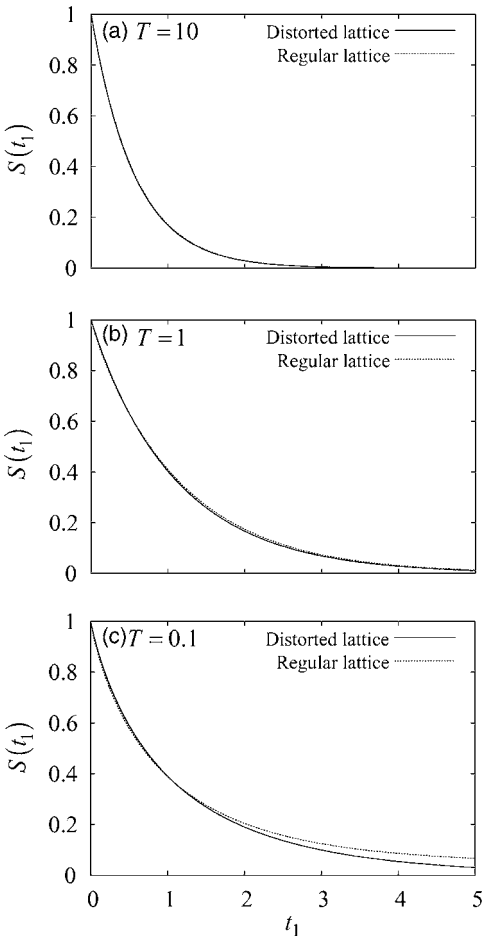

FIG. 9. The 1D signals calculated from the Smoluchowski approach for the FEL given in Figs. 2(a)–2(f): (a) $T=10$ for the high temperature case, (b) $T=1$ for the middle temperature case, and (c) $T=0.1$ for the low temperature case. In each figure, the solid and dotted lines represent the distorted and regular lattice cases, respectively.

The 2D signals are presented in Figs. 10(a)–10(f). As mentioned in Sec. V, the 2D signals in the high temperature case arise from the nonlinearity of the dipole elements. If we calculate the 2D signals with setting $\varepsilon=0$ for a harmonic potential with quartic anharmonicity using the Smoluchowski equation, the signal becomes negative with a different 2D profile (not shown). This fact supports the form of dipole given in Eq. (6.3). While the Smoluchowski equation well reproduces the 1D signals at all temperatures and the 2D signals at high temperature calculated from the master equation, it cannot simulate the 2D signals in the low

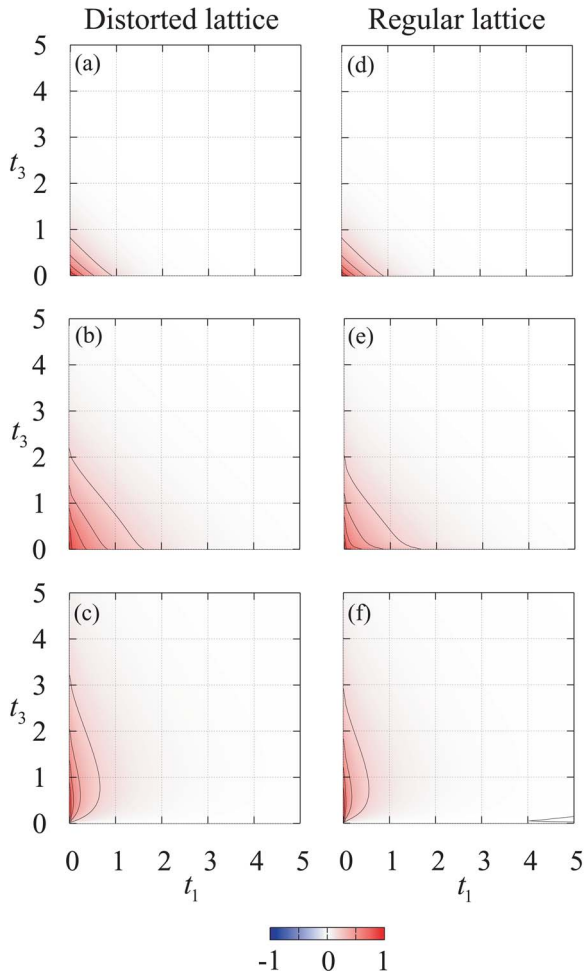

FIG. 10. (Color online) The contour maps of the 2D signals calculated from the Smoluchowski equation with the nonlinear excitation for the distorted cases [(a)–(c)], and the regular lattice cases [(d)–(f)], at different temperatures in the same order of Figs. 2(a)–2(f). The intensity of each plot is normalized by its maximum.

temperature cases, as shown in Figs. 10(b), 10(c), 10(e), and 10(f). For these figures, we use the same relaxation constant D as in the dashed and solid lines of Figs. 9(a)–9(c), but even we change D as well as the nonlinearlity of dipole ε we cannot reproduce similar profiles in Figs. 6(b), 6(c), 6(e), and 6(f). This result indicates that the applicability of the Smoluchowski equation is limited to the high temperature case, where the FEL profile is parabolic. We should address that this limitation becomes prominent due to the sensitivity of 2D spectroscopy.

VII. CONCLUSIONS

By employing a simple model of the regular and distorted dipolar system which allows us to have the exact FEL and collective dynamics of the system at any temperatures, we explored a possibility to obtain information on the FEL by spectroscopic means. The evaluated FEL exhibits the parabolic shape at high temperature, whereas it shows a bumpy profile with some minima at low temperature, where the motion of dipoles is frozen. From the master equation approach, we calculated the 1D and 2D singles for single flip and single-double flips dynamics. While the 1D signals were characterized by the featureless exponential or sum of exponential relaxation signals regardless of the FEL profiles, 2D spectra showed distinct differences for different FEL profiles. The local minima of the FEL were detected as the elongation of 2D signals in the t_3 direction. This indicates that 2D spectroscopy may be a useful tool to analyze the FEL profile expressed as the function of system polarization.

To examine the validity of Smoluchowski equation, we also calculated the 1D and 2D spectra using the microscopically calculated FELs. For the high temperature case, the dynamics described by the master equation and Smoluchowski equation was essentially the same for the large system and the calculated 1D and 2D signals were the same. However, in the middle and low temperature cases, these signals were different, which indicates that Smoluchowski equation might not be accurate to describe the dynamics for the system with nonparabolic FELs.

Finally, we should address the limitation of the present analysis. To have the accurate FEL with the decreasing the degrees of freedom, we had to discretize the configuration of dipoles which made impossible to employ kinetic dynamics. We thus employ the stochastic dynamics using the master equation. To make the statement more concrete, we have to compare the present results with the kinetic ones. For instance, although the Smoluchowski equation reproduces the stochastic results only in the high temperature case, this statement may change if we consider the kinetic system. The model dependence as well as the size dependence of the present results have not been explored, which is essential to discuss a real system.

ACKNOWLEDGMENTS

Y.T. thanks to Japan Society for the Promotion of Science for the support of this work under the Grant-in-Aid for Scientific Research A 15205005. Y.S. is supported by the research fellowship of Global COE program, International Center for Integrated Research and Advanced Education in Material Science, Kyoto University, Japan.

APPENDIX A: DERIVATION OF THE SMOLUCHOWSKI EQUATION

In this appendix, we discuss the relation between the master equation and the Smoluchowski equation.[25] The time evolution of our system is given by the master equation Eq. (3.1), and the probability distribution vector $\boldsymbol{\rho}(t)$ has 2^N states. Here we rewrite the Eq. (3.1) as the following form:

$$\frac{\partial}{\partial t}\rho_i(t) = \sum_j [(-\mathbf{L})_{i,j}\rho_j(t) - (-\mathbf{L})_{j,i}\rho_i(t)]. \tag{A1}$$

For the high temperature case, the transition occurs absolutely if two states are connected with given dynamics, thus the transition matrix, $-\mathbf{L}=-\alpha\mathbf{L}^{(1)}-\beta\mathbf{L}^{(2)}$, can be written as

$$(-\mathbf{L})_{i,j} = \alpha C^{(1)}_{i,j} + \beta C^{(2)}_{i,j}, \tag{A2}$$

where $C_{i,j}^{(n)}$ is the connectivity coefficient introduced in Sec. III. Assuming a single flip and double flips of dipole in the system whose polarization is P_j, we can construct the rate equation expressed as

$$\frac{\partial}{\partial t}\rho_{i,P_i}(t) = -\alpha N\rho_{i,P_i}(t) - \beta\frac{N(N-1)}{2}\rho_{i,P_i}(t) + \alpha\sum_j \rho_{j,P_j}(t)C_{i,j}^{(1)}\delta(P_i - \{P_j - \Delta P\}) + \alpha\sum_j \rho_{j,P_j}(t)C_{i,j}^{(1)}\delta(P_i - \{P_j + \Delta P\}) + \beta\sum_j \rho_{j,P_j}(t)C_{i,j}^{(2)}\delta(P_i - \{P_j - 2\Delta P\}) + \beta\sum_j \rho_{j,P_j}(t)C_{i,j}^{(2)}\delta(P_i - P_j) + \beta\sum_j \rho_{j,P_j}(t)C_{i,j}^{(2)}\delta(P_i - \{P_j + 2\Delta P\}), \tag{A3}$$

where $\rho_{i,P_i}(t)$ is the ith component of the probability distribution vector $\boldsymbol{\rho}(t)$ and the subscript P_i is introduced for representing the polarization of the ith state. Here we calculate the polarization and time probability distribution function $H(P(k),t)$ by summing Eq. (A3) over all states with the same polarization $P(k)$. Operating $\Sigma_i\delta_{P(k),P_i}$ to both sides of Eq. (A3), we obtain

$$\frac{\partial}{\partial t}H(P(k),t) = -\left[\alpha N + \beta\left(\frac{N^2}{4} - \frac{N}{2} + k^2\right)\right]H(P(k),t) + \alpha\left(\frac{N}{2} + 1 - k\right)H(P(k) - \Delta P,t) + \alpha\left(\frac{N}{2} + 1 + k\right)H(P(k) + \Delta P,t) + \beta\left\{\frac{N^2}{8} + \frac{3N}{4} + 1 + \frac{1}{2}[k^2 - k(N+3)]\right\}H(P(k) - 2\Delta P,t) + \beta\left\{\frac{N^2}{8} + \frac{3N}{4} + 1 + \frac{1}{2}[k^2 + k(N+3)]\right\}H(P(k) + 2\Delta P,t). \tag{A4}$$

Here, assuming $P(k)$ be continuous variable and taking large N limit, we get

$$\frac{\partial}{\partial t}H(P,t) = \left(\gamma\frac{\partial}{\partial P}P + D\frac{\partial^2}{\partial P^2}\right)H(P,t), \tag{A5}$$

where we set $\gamma = 2(\alpha + N\beta)$ and $D = N\Delta P^2(\alpha + N\beta)/2$. The first and second terms correspond to the drift term and diffusion terms, respectively.

APPENDIX B: LINEAR ABSORPTION SIGNAL FROM SMOLUCHOWSKI EQUATION APPROACH

If the potential is harmonic, the Smoluchowski equation for a given arbitrary initial condition can be easily solved as

$$H(P,t) = \sum_{n=0} a_n \exp(-n\gamma t)\exp\left(-\frac{\gamma}{2D}P^2\right)H_n\left(\sqrt{\frac{\gamma}{2D}}P\right), \tag{B1}$$

where $H_n(\xi)$ are the Hermite polynomials and a_n are the initial values for nth eigenfunctions. For 1D spectroscopy, the nonlinearity of dipole plays a minor role, so we can set $\varepsilon = 0$ in Eq. (6.3). At high temperature, the FEL is approximated by parabolic function, so that the initial condition of the Smoluchowski immediately after excitation is expressed by the first Hermite polynomial, i.e., $H(P,0) \sim \exp(-\xi^2)H_1(\xi)$, where $\xi = \sqrt{\gamma/2D}P$. Thus, the 1D signal for high temperature is analytically evaluated as

$$S(t_1) \sim \exp(-\gamma t)\int dP \exp\left(-\frac{\gamma}{2D}P^2\right)H_1\left(\sqrt{\frac{\gamma}{2D}}P\right). \tag{B2}$$

This equation indicates the signal decays exponentially as the relaxation of collective mode with the relaxation rate γ.

[1] C. A. Angell, K. L. Ngai, G. B. McKenna, P. F. McMillan, and S. W. Martin, J. Appl. Phys. **88**, 3113 (2000).
[2] P. Welch and M. Muthukumar,. Phys. Rev. Lett. **87**, 218302 (2001).
[3] R. A. Marcus, Rev. Mod. Phys. **65**, 599 (1993).
[4] C. L. Brooks III, M. Gruebele, J. N. Onuchic, and P. G. Wolynes, Proc. Natl. Acad. Sci. U.S.A. **95**, 11037 (1998).
[5] D. J. Wales, *Energy Landscapes* (Cambridge University Press, Cambridge, 2003).
[6] D. J. Wales and T. V. Bogdan, J. Phys. Chem. B **110**, 20765 (2006).
[7] L. D. Landau, Phys. Z. Sowjetunion **11**, 26 (1937); **11**, 545 (1937).
[8] M. Mezard, G. Parisi, and M. A. Virasoro, *Spin Glass Theory and Beyond* (World Scientific, Singapore, 1987).
[9] M. Cyrot, Rep. Prog. Phys. **36**, 103 (1973).
[10] K. Kawasaki, M. C. Yalabik, and J. D. Gunton, Phys. Rev. A **17**, 455 (1978).
[11] S. Noguchi and T. Ohta, J. Phys. Soc. Jpn. **72**, 1315 (2003).
[12] D. F. Calef and P. G. Wolynes, J. Chem. Phys. **78**, 470 (1983).
[13] J. K. Hwang and A. Warshel, J. Am. Chem. Soc. **109**, 715 (1987).
[14] R. A. Kuharski, J. S. Bader, D. Chandler, M. Sprik, M. L. Klein, and R. W. Impey, J. Chem. Phys. **89**, 3248 (1988).
[15] E. A. Carter and J. T. Hynes, J. Phys. Chem. **93**, 2184 (1989).
[16] K. Ando and S. Kato, J. Chem. Phys. **95**, 5966 (1991).
[17] L. D. Zusman, Chem. Phys. **49**, 295 (1980).
[18] B. Bagchi, G. R. Fleming, and D. W. Oxtoby, J. Chem. Phys. **78**, 7375 (1983).
[19] N. Agmon and J. J. Hopfield, J. Chem. Phys. **78**, 6947 (1983).
[20] H. Sumi and R. A. Marcus, J. Chem. Phys. **84**, 4272 (1986).

[21] K. Seki, A. V. Barzykin, and M. Tachiya, J. Chem. Phys. **110**, 7639 (1999).
[22] B. Bagchi and N. Gayathri, Adv. Chem. Phys. **107**, 1 (1999).
[23] K. Ando and H. Sumi, J. Chem. Phys. **118**, 8315 (2003).
[24] J. N. Onuchic and P. G. Wolynes, J. Chem. Phys. **98**, 2218 (1993).
[25] V. B. P. Leite and J. N. Onuchic, J. Phys. Chem. **100**, 7680 (1996).
[26] Y. Tanimura, V. B. P. Leite, and J. N. Onuchic, J. Chem. Phys. **117**, 2172 (2002).
[27] V. B. P. Leite, L. C. P. Alonso, M. Newton, and J. Wang, Phys. Rev. Lett. **95**, 118301 (2005).
[28] Y. Suzuki and Y. Tanimura, J. Chem. Phys. **124**, 124508 (2006).
[29] Y. Suzuki and Y. Tanimura, J. Chem. Phys. **126**, 054504 (2007).
[30] G. Diezemann, U. Mohanty, and I. Oppenheim, Phys. Rev. E **59**, 2067 (1999).
[31] T. Yoshidome, A. Yoshimori, and T. Odagaki, Phys. Rev. E **76**, 021506 (2007).
[32] G. Adjanor, M. Athenes, and F. Calvo, Eur. Phys. J. B **53**, 47 (2006).
[33] P. Welch and M. Muthukumar, Phys. Rev. Lett. **87**, 218302 (2001).
[34] N. Go and H. A. Scheraga, Macromolecules **9**, 535 (1976).
[35] A. Kitao, S. Hayward, and N. Go, Proteins **33**, 496 (1998).
[36] A. Kitao and N. Go, Curr. Opin. Struct. Biol. **9**, 164 (1999).
[37] D. A. Evans and D. J. Wales, J. Chem. Phys. **119**, 9947 (2003).
[38] J. N. Onuchic, Z. Luthey-Schulten, and P. G. Wolynes, Annu. Rev. Phys. Chem. **48**, 545 (1997).
[39] J.-E. Shea, J. N. Onuchic, and C. L. Brooks III, Proc. Natl. Acad. Sci. U.S.A. **99**, 16064 (2002).
[40] P. Weinkam, C. Zong, and P. G. Wolynes, Proc. Natl. Acad. Sci. U.S.A. **102**, 12401 (2005).
[41] N. Go, Annu. Rev. Biophys. Bioeng. **12**, 183 (1983).
[42] J. N. Onuchic and P. G. Wolynes, Curr. Opin. Struct. Biol. **14**, 70 (2004).
[43] Y. Sugita, A. Kitao, and Y. Okamoto, J. Chem. Phys. **113**, 6042 (2000).
[44] M. Leitgeb, C. Schröder, and S. Boresch, J. Chem. Phys. **122**, 084109 (2005).
[45] W. T. Coffey, Y. P. Kalmykov, and J. T. Waldron, *The Langevin Equation* (World Scientific, Singapore, 1996).
[46] R. J. Glauber, J. Math. Phys. **4**, 294 (1963).
[47] N. Go, J. Stat. Phys. **30**, 413 (1983).
[48] B. A. Patel, P. G. Debenedetti, and F. H. Stillinger, J. Phys. Chem. A **111**, 12651 (2007).
[49] J. M. Luttinger and L. Tisza, Phys. Rev. **70**, 954 (1946).
[50] D. V. Matyushov, J. Chem. Phys. **120**, 1375 (2004).
[51] Y. Tanimura and S. Mukamel, J. Chem. Phys. **99**, 9496 (1993).
[52] P. Hamm, M. Lim, and R. M. Hochstrasser, J. Phys. Chem. B **102**, 6123 (1998).
[53] Y. Tanimura, J. Phys. Soc. Jpn. **75**, 082001 (2006).
[54] K. Okumura, A. Tokmakoff, and Y. Tanimura, Chem. Phys. Lett. **314**, 488 (1999).
[55] K. Okumura, D. M. Jonas, and Y. Tanimura, Chem. Phys. **266**, 237 (2001).
[56] S. Hahn, K. Kwak, and M. Cho, J. Chem. Phys. **112**, 4553 (2000).
[57] Y. Nagata, Y. Tanimura, and S. Mukamel, J. Chem. Phys. **126**, 204703 (2007).
[58] N. Demirdoven, M. Khalil, and A. Tokmakoff, Phys. Rev. Lett. **89**, 237401 (2002).
[59] K. A. Merchant, W. G. Noid, D. E. Thompson, R. Akiyama, R. F. Loring, and M. D. Fayer, J. Phys. Chem. B **107**, 4 (2003).
[60] K. F. Everitt, E. Geva, and J. L. Skinner, J. Chem. Phys. **114**, 1326 (2001).
[61] Y. Tanimura and K. Okumura, J. Chem. Phys. **106**, 2078 (1997).
[62] A. Ishizaki and Y. Tanimura, J. Chem. Phys. **125**, 084501 (2006).
[63] Y. Suzuki and Y. Tanimura, J. Chem. Phys. **119**, 1650 (2003).
[64] K. Okumura and Y. Tanimura, Chem. Phys. Lett. **295**, 298 (1998).
[65] S. Mukamel, *Principles of Nonlinear Optical Spectroscopy* (Oxford University Press, New York, 1995).
[66] T. Steffen and Y. Tanimura, J. Phys. Soc. Jpn. **69**, 3115 (2000); **76**, 078001 (2007).
[67] Y. Tanimura and T. Steffen, J. Phys. Soc. Jpn. **69**, 4095 (2000).
[68] T. Kato and Y. Tanimura, J. Chem. Phys. **117**, 6221 (2002).
[69] T. Kato and Y. Tanimura, J. Chem. Phys. **120**, 260 (2004).
[70] T. Hasegawa and Y. Tanimura, J. Chem. Phys. **128**, 064511 (2008).
[71] H. Takano and S. Miyashita, J. Phys. Soc. Jpn. **64**, 3688 (1995).
[72] S. Koseki, H. Hirao, and H. Takano, J. Phys. Soc. Jpn. **66**, 1631 (1997).